

Water diffusion through a membrane protein channel: A first passage time approach

Vincent J. van Hijkoop, Anton J. Dammers,^{a,b)}
Kourosh Malek, and Marc-Olivier Coppens^{a,c)}

*Physical Chemistry and Molecular Thermodynamics, DelftChemTech, Delft University of Technology,
Julianalaan 136, 2628 BL Delft, The Netherlands*

(Received 4 May 2007; accepted 26 June 2007; published online 28 August 2007)

Water diffusion through OmpF, a porin in the outer membrane of *Escherichia coli*, is studied by molecular dynamics simulation. A first passage time approach allows characterizing the diffusive properties of a well-defined region of this channel. A carbon nanotube, which is considerably more homogeneous, serves as a model to validate the methodology. Here we find, in addition to the expected regular behavior, a gradient of the diffusion coefficient at the channel ends, witness of the transition from confinement in the channel to bulk behavior in the connected reservoirs. Moreover, we observe the effect of a kinetic boundary layer, which is the counterpart of the initial ballistic regime in a mean square displacement analysis. The overall diffusive behavior of water in OmpF shows remarkable similarity with that in a homogeneous channel. However, a small fraction of the water molecules appears to be trapped by the protein wall for considerable lengths of time. The distribution of trapping times exhibits a broad power law distribution $\psi(\tau) \sim \tau^{-2.4}$, up to $\tau=10$ ns, a bound set by the length of the simulation run. We discuss the effect of this distribution on the dynamic properties of water in OmpF in terms of incomplete sampling of phase space. © 2007 American Institute of Physics. [DOI: 10.1063/1.2761897]

I. INTRODUCTION

Nanometer-sized transmembrane protein channels play a pivotal role in the diffusive transport of water, ions, and other species between biological cells and their environment. One particular channel protein that has received much attention is the OmpF porin,^{1–4} an aqueous pore that is found in the outer membrane of *Escherichia coli*. In its natural form OmpF is a trimer, i.e., it consists of three similar parallel channels in a triangular arrangement (see Fig. 1). The internal region of an OmpF channel, accessible by liquid, has the shape of an hourglass. The channel diameter decreases from 2 nm near the channel ends to approximately 0.6 nm in the constriction zone.² Molecular dynamics (MD) simulations have given substantial insight into the relation between channel structure and transport properties of water and solvents. Charged residues in the pore wall are responsible for preferential orientation of water molecules² and separated pathways for positive and negative ions, respectively.^{3,4} The axial diffusion coefficient, which characterizes the component of the molecular motion parallel to the channel axis, appears to be strongly position dependent, for water² as well as for ions.³ Typically a reduction of the water diffusion coefficient by a factor of 5 was observed,² moving from the bulk liquid toward the constriction zone. The spatial variation of diffusion characteristics makes the transition from local properties to full-channel behavior nontrivial.

In a homogeneous isotropic simple fluid the mean square displacement (MSD) of a molecule in a particular direction, say z , is given by the Einstein relation,

$$\lim_{t \rightarrow \infty} \langle [z(t) - z(0)]^2 \rangle = 2Dt, \quad (1)$$

where t is time, D is the self-diffusion coefficient, and $z(0)$ and $z(t)$ are the z components of the particle positions at times 0 and t , respectively. This expression is valid for times considerably longer than the velocity correlation time, i.e., well beyond the initial ballistic regime, where the MSD is proportional to t^2 . Equation (1) would also apply to axial diffusion in a translationally invariant channel. If heteroge-

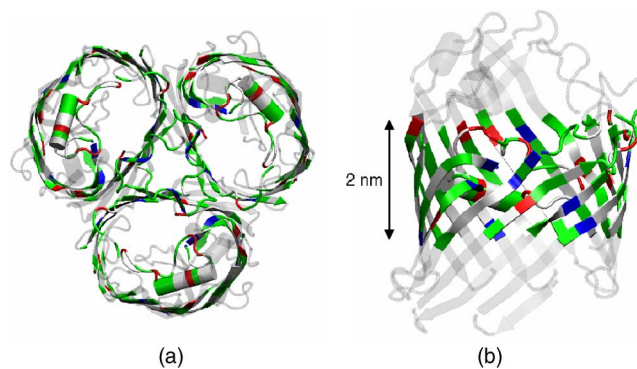


FIG. 1. (Color online) Visualization of the protein structure of OmpF. 7 (a) Top view of the trimer. (b) Side view of a single channel. It has a cylindrical shape, built out of beta sheets. The helix in the center (L3 loop) is responsible for a strong transverse electric field (Ref. 2). The 2 nm long region of the channel that was used in the analysis is emphasized. The figures were generated with VMD (Ref. 28).

^{a)} Authors to whom correspondence should be addressed.

^{b)} Electronic mail: a.j.dammers@tudelft.nl

^{c)} Also at Isermann Department of Chemical and Biological Engineering, Rensselaer Polytechnic Institute, Troy, NY 12180. Electronic mail: m.o.coppens@tudelft.nl

neities are present, the limiting linear behavior will only be reached after these are sufficiently sampled, yielding a diffusion coefficient that represents an average over the explored region. The intermediate time dependence of the MSD will then, in general, be nonlinear. As the typical length scale of the heterogeneities in OmpF is of the same order of magnitude as the channel length, extracting an effective diffusion coefficient from the Einstein relation [Eq. (1)] is not a viable option. Trajectories sampling the heterogeneities in a sufficiently representative manner would extend well into the embedding water reservoir, which obscures the effect of the intrinsic channel properties on the MSD in an intractable way.

Deviations of the MSD from the linear time dependence [Eq. (1)] may arise simply due to the presence of bounding surfaces, even when the liquid has uniform intrinsic properties. This feature was accounted for analytically in several MD studies of water⁵⁻⁷ through mapping onto simple geometries, where surfaces are represented by reflecting boundaries. From the solution of the diffusion equation finite-time corrections to the MSD [Eq. (1)], related to diffusion in a direction perpendicular to the surface, could be derived. The modified expressions were then used to extract intrinsic diffusion coefficients from the MD simulation results. Examples of this approach are diffusion of water near a protein surface, represented by a plane bounding a semi-infinite domain,⁵ between amphiphilic layers, represented by parallel planes,⁶ and within a silica tube, modeled as a cylinder.⁷

In OmpF, nonlinearity of the MSD of water is the result of variations of the channel cross section as well as interactions of the water molecules with the protein residues which form the channel wall. This means that a combination of geometry-induced and intrinsic variations of the diffusion characteristics plays a role. Tieleman and Berendsen² used the Einstein relation [Eq. (1)] in the three principal directions to retrieve the components of the *local* diffusion tensor from MD simulation data by considering thin (1.2 Å) slices perpendicular to the channel (z) axis. Molecules present in a particular slice at time zero are monitored during a time interval of 5 ps, of which only the last 4 ps are used in order to be well beyond the ballistic regime. The effective diffusion coefficients related to the slice, D_x , D_y , and D_z , respectively, are then extracted from linear fits to the MSD(t) curves, obtained for multiple time origins and averaged over all molecules initially in the slice. The short time interval ensures that molecules travel distances which are small relative to the typical length scale of variations in the channel cross section. In other words, the obtained approximate diffusion coefficients represent (radially averaged) intrinsic liquid properties. A similar approach was followed for the analysis of ionic diffusion in OmpF (Ref. 3) as well as in various other ion channels.⁸ A related methodology was applied earlier by Ahlström *et al.*⁹ to water diffusion in 1-Å-thick concentric spherical shells around a globular protein. Here, the full time-dependent solution of the diffusion equation, rather than the MSD, was analyzed to extract radial diffusion coefficients from the simulations.

In the layer-based approaches summarized above, the initial positions of the molecules are known, but averaging

takes place over poorly defined regions, which extend beyond the boundaries of the layers. Liu *et al.*¹⁰ alleviated this limitation in a study of the diffusive properties of water in layers of thickness of 3.5 Å parallel to a liquid-vapor interface. In this approach the two delineating surfaces of a layer are treated as virtual absorbing boundaries. All molecules present in the layer at time zero are labeled and lose their identities upon crossing a boundary at some later time. The diffusion coefficient of a layer is obtained from the MD simulation data by matching the decay of the concentration of tagged molecules to the solution of the diffusion equation with absorbing boundary conditions. A related method was applied by Munakata and Kaneko.¹¹ They monitored the time it takes a molecule to reach a sphere of radius l around its initial position for the first time. This is a typical example of a first passage time (FPT) problem.¹² Essentially, it amounts again to solving the diffusion equation for the concentration $c(\mathbf{r}, t)$, with absorbing boundary conditions at $|\mathbf{r}|=l$ and initial concentration $c(\mathbf{r}, 0)=\delta(\mathbf{r})$, but rather than the explicit solution, a characteristic time is the quantity of interest. In this spherical model the initial position of the molecule is symmetric with respect to the boundary. Variation of this position, however, would allow for a much richer analysis of the diffusion behavior. Recently,¹³ we applied such a more general methodology to various liquids in a rectangular geometry, where slabs of thickness of 2 nm within a larger simulation box were analyzed. The diffusion coefficients obtained along this line showed good agreement with the values found by means of a regular MSD analysis [Eq. (1)]. However, the analysis unambiguously forced us to assume an *effective* slab thickness that exceeded the actual distance between the absorbing boundaries. That is, boundaries appeared as being shifted outwards over a distance λ_M . This quantity, which appeared to vary with type of molecule and simulation conditions, was identified as the “Milne extrapolation length.”¹⁴ It has the same physical background as the more familiar initial ballistic regime preceding the diffusive behavior [Eq. (1)]. This phenomenon was revealed by varying the initial particle position. Such a feature renders the FPT method particularly promising for the analysis of molecular diffusion through heterogeneous channels. Permeation times of particles entering the channel at one side and leaving it at the other provide a global (effective) characterization of the system. Exit times of particles which start from some internal position are expected to be especially influenced by local properties. Here we present the results of such a FPT analysis to water diffusing through an OmpF channel, and, as a simplified model system thereof, a carbon nanotube.

This paper is organized as follows. In Sec. II we give computational details and parameters of the MD simulations. Section III provides the mathematical ingredients of the FPT analysis. In Sec. IV A we apply these to water diffusing through a carbon-nanotube-like cylindrical channel. This serves as a validation of the proposed methodology and also as a reference system for the more complicated OmpF channel. Section IV B presents the analysis of OmpF MD simulations. Distinct features clearly reveal the heterogeneous nature of the channel, but the global permeation behavior

appears to be remarkably similar to that of a homogeneous channel, governed by a single effective diffusion coefficient. In Sec. V we summarize the main conclusions.

II. SIMULATION METHODOLOGY AND PARAMETERS

Molecular dynamics simulations were carried out using the software package GROMACS.¹⁵

Water model. A modified version of the simple point charge (SPC) model¹⁶ was used to represent the water molecules in both simulations. Here the mass of the two hydrogen atoms in a molecule is multiplied by a factor of 4, which is compensated by a reduction of the oxygen mass accordingly. The motivation¹⁶ for this unphysical redistribution of masses is an increase of the moments of inertia of the water molecules. This results in suppression of high-frequency librations, allowing us to take a larger time step in the integration of the equations of motion. A side effect of this procedure, however, is slowing down of the global rotational motion of the molecules as well. Due to the strong rotation-translation coupling, as a result of hydrogen bonding, this has a considerable impact on their translational diffusion. Typically, the diffusion coefficient appears to be reduced by roughly 15% relative to the regular SPC water model. Variations of diffusion coefficients between various frequently used water models, however, are of the same order of magnitude, if not larger.¹⁷ Therefore, we consider the modified SPC water model to be an acceptable choice.

Carbon nanotube. The behavior of water was analyzed in an open-ended rigid (12,12)-type carbon nanotube (CNT), with a length of 2.7 nm and an approximate internal diameter of 1.2 nm. This channel is placed symmetrically, parallel to the z axis, in a simulation box with dimensions $L_x \times L_y \times L_z = 5.1 \times 5.1 \times 6.0$ nm³. Two parallel graphite sheets, perpendicular to the channel, with spacing of 2.7 nm, separate two water reservoirs. A connection between these reservoirs is provided by the CNT. Polarizability of the carbon atoms was not taken into account, and, therefore, the results presented here are of limited significance to real CNT's. Rather, we choose this system as a generic hydrophobic channel. Atomic arrangements of the CNT and the graphite sheets were obtained using the web-based applets TubeGen and PRODRG.^{18,19} The system contains 7076 atoms in total.

OmpF. The molecular structure of OmpF was retrieved from a publicly accessible online database [RCSB Protein Databank, PDB ID: 2OMF, resolution of 2.4 Å (Refs. 1 and 20)]. OmpF consists of three parallel channels (see Fig. 1). This system is embedded in a dimyristoylphosphatidylcholine (united atom) bilayer, surrounded by SPC water. Dimensions of the simulation box are $L_x \times L_y \times L_z = 12.4 \times 12.4 \times 8.0$ nm³. The total number of atoms in the simulation amounts to 93 009.

Simulation settings. The GROMACS *ffgm*x force field was used in both simulations, in conjunction with united-atom lipid molecules, dummy hydrogen atoms for the protein, and the mentioned modification to the SPC water model.¹⁶ Periodic boundary conditions were applied in three dimensions. Long-range electrostatics was accounted for by means of particle-mesh Ewald summation. Short-range van der Waals

and Coulombic interactions were calculated, with cutoff lengths of 1.0 and 0.9 nm for the CNT simulation and the OmpF simulation, respectively. Both systems were coupled to a Berendsen thermostat at 310 K.²¹ Berendsen pressure coupling was applied at 1 bar in the OmpF simulation. All (classical) degrees of freedom of OmpF were taken into account explicitly. In the CNT simulation, pressure coupling caused severe deformations of the graphite sheets. Therefore it was replaced by position restraints by applying a force of 1000 kJ/mol nm² to each carbon atom. Box dimensions were kept fixed during this simulation.

The time steps used for integrating the equations of motion were 2 fs for the CNT simulations and 5 fs for the simulations on OmpF. In the latter case, a larger time step was chosen for reasons of computational efficiency. This was allowed due to a different treatment of the hydrogen atoms involved in the simulation. Lengths of production runs were 20 and 10 ns for a CNT and OmpF, respectively.

III. FIRST PASSAGE TIME APPROACH

For diffusion through a channel, the component of the molecular motion projected on the channel (z) axis is the quantity of primary interest. If the channel has a z -independent (geometrical and chemical) structure, this longitudinal component is decoupled from the transversal one, so a truly one-dimensional description would apply. Heterogeneities in the channel, such as in OmpF, may give rise to deviations from this simple behavior. These can then be used to gain insight into the effect of the channel's architecture on the diffusion properties. As discussed in the Introduction, the finite size of a channel limits the use of the Einstein relation [Eq. (1)] for the determination of a diffusion coefficient from simulation data. This problem, however, can be circumvented by a first passage time analysis. In this section we present the relevant associated mathematical expressions for a homogeneous one-dimensional diffusion model. Details pertaining to their derivation are discussed in Ref. 13, while a much more comprehensive account of the FPT methodology, including an extensive list of references to the original literature, can be found in a book by Redner.¹²

We consider diffusion of particles on a one-dimensional interval $[0, L]$, with absorbing boundaries at $z=0$ and $z=L$, respectively. This model represents the z -projected motion of molecules in a channel of length L , delimited by virtual boundaries, i.e., molecules lose their identity when crossing a boundary, but are not physically removed from the system. Starting point is Fick's law, which relates a diffusion current density $j(z, t)$ on time t and position z to a concentration gradient as

$$j(z, t) = -D \frac{\partial}{\partial z} c(z, t), \quad (2)$$

where $c(z, t)$ is the particle concentration and D is the diffusion coefficient. Application of the continuity equation then leads to the diffusion equation,²²

$$\frac{\partial}{\partial t} c(z, t) = D \frac{\partial^2}{\partial z^2} c(z, t). \quad (3)$$

Absorbing boundary conditions are imposed by the requirement

$$c(0, t) = c(L, t) = 0. \quad (4)$$

Although Eq. (2) is a transport equation, the diffusion coefficient D should be interpreted as the *self* (tracer)-diffusivity. This emerges because in the computational “experiments” we consider individual, labeled, particles. Global properties are obtained by first averaging over individual trajectories, and subsequently over the ensemble of trajectories comprising the full system. This bypasses any correlations between the dynamics of the particles, i.e., they are treated as noninteracting. Under this condition the transport diffusivity is equal to the self-diffusivity.

The time dependent spatial distribution of particles launched at time $t=0$, and position $z=z_0$ within the domain $[0, L]$ corresponds to the solution of Eq. (3) with the initial condition $c(z, 0) = \delta(z-z_0)$ as²²

$$c(z, t) = \frac{2}{L} \sum_{n=1}^{\infty} \sin\left(\frac{n\pi z_0}{L}\right) \sin\left(\frac{n\pi z}{L}\right) e^{-t/\tau_n}, \quad (5)$$

where time constants τ_n are defined as

$$\tau_n = \frac{L^2}{n^2 \pi^2 D}. \quad (6)$$

The mean exit time, i.e., the average time it takes a particle to reach either boundary, given an initial position z_0 , can be derived from Eq. (5) as

$$T(z_0) = \frac{1}{2D} z_0(L - z_0). \quad (7)$$

This is a parabola, which reaches a maximum value $L^2/8D$ at $z_0=L/2$ and crosses the z_0 axis at $z_0=0$ and $z_0=L$, respectively. The area under this curve gives the *spatially averaged* mean exit time $\langle T \rangle$, which corresponds to a uniform initial distribution, rather than a delta pulse, as

$$\langle T \rangle = \frac{1}{L} \int_0^L T(z_0) dz_0 = \frac{L^2}{12D}. \quad (8)$$

Of particular interest for application of the FPT methodology to diffusion through channels is the distribution of permeation times $F_p(t)$, which characterizes the residence time of particles that enter the channel at one end, and are absorbed at the other end (and, therefore, never return to the entrance at intermediate times). It is given by the series expansion

$$F_p(t) = \frac{2\pi^2 D}{L^2} \sum_{n=1}^{\infty} (-1)^{n-1} n^2 e^{-t/\tau_n}. \quad (9)$$

The fraction of particles that have entered the interval at $t=0$ and eventually will leave it at the opposite end, but have not done so yet at time t , is given by the *survival probability* $S_p(t)$, which is equal to the complementary cumulative permeation time distribution

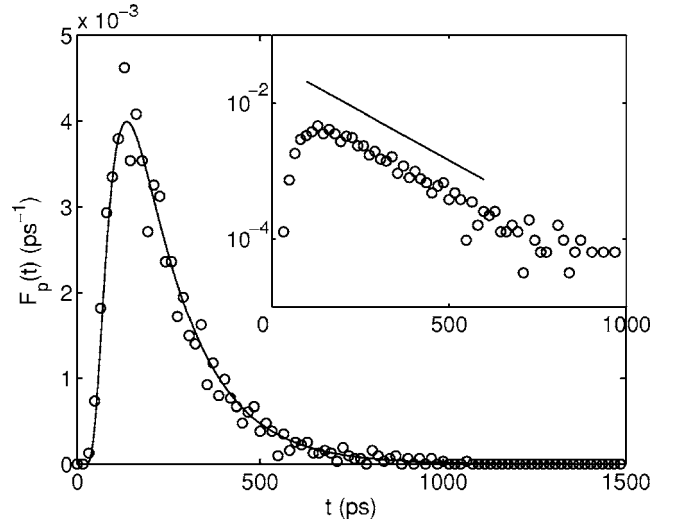


FIG. 2. Permeation time distribution $F_p(t)$ of water molecules traversing a CNT of length $L=2$ nm. The solid curve is based on Eq. (9), with $D=2.70$ nm²/ns, obtained from the fit in Fig. 3. The solid line in the semi-logarithmic inset emphasizes the asymptotic monoexponential behavior, with a time constant $\tau_1=L^2/\pi^2 D$.

$$S_p(t) = \int_t^{\infty} F_p(t') dt' = 2 \sum_{n=1}^{\infty} (-1)^{n-1} e^{-t/\tau_n}. \quad (10)$$

While formally $S_p(t)$ contains the same information as $F_p(t)$, it proved to be useful for the analysis of MD simulation data. $F_p(t)$ is given by Eq. (9) as a sum of exponential terms $a_n e^{-t/\tau_n}$. Integration of such a term generates a prefactor $\tau_n \sim n^{-2}$ [Eq. (6)], so the high- n contributions are reduced relative to the low- n ones. This is a manifestation of the well-known fact that integration acts as a low-pass filter. The latter property is responsible for the suppression of statistical fluctuations upon transformation from $F_p(t)$ to $S_p(t)$.

IV. RESULTS

A. Carbon nanotube

Carbon nanotubes have been the subject of much computational research, as model systems for the study of transport through nanopores, as well as in their own right (see, e.g., Refs. 23–25). We examine diffusion of water in a CNT of length of 2.7 nm and an approximate internal diameter of 1.2 nm, as a prelude to the heterogeneous OmpF channel. The “computational length” L , which defines the region over which the FPT analysis is applied, is 2 nm. It is positioned symmetrically in the channel. A simulation run of 20 ns was analyzed using multiple time origins.

Figure 2 shows the permeation time distribution function $F_p(t)$, which characterizes the time it takes a molecule to cross the channel without returning to its entrance plane at intermediate times. The model system contains 1746 water molecules, but on average typically only 80 are present in the CNT. Therefore, most of the computational work consists of updating the water reservoirs connected by the channel, whereas only less than 5% of the water molecules provide information of interest. This causes the considerable statistical fluctuations in Fig. 2. As argued in Sec. III, these fluctuations

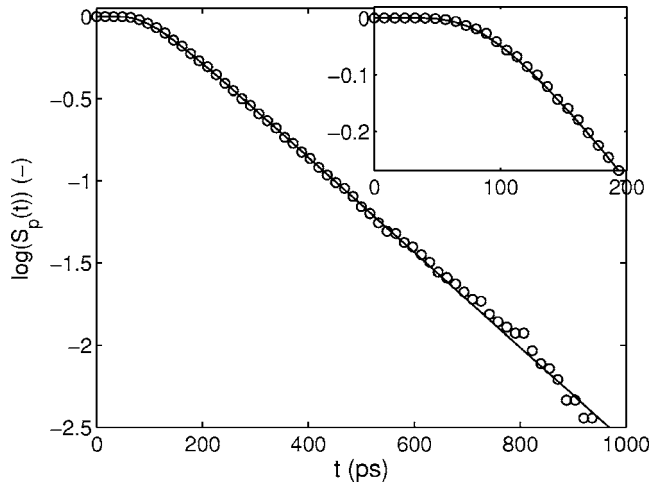


FIG. 3. Survival probability $S_p(t)$ of water molecules traversing a CNT of length $L=2$ nm. The solid curve (—) is based on Eq. (10), with $D=2.70$ nm²/ns. The inset shows the initial part of the curve in more detail.

tuations may be suppressed by transforming the data into the survival probability $S_p(t)$ [Eq. (10)]. Figure 3 shows that this is indeed the case. The asymptotic (long time) linear part of $S_p(t)$ corresponds to the ($n=1$) term in Eq. (10), governed by a time constant $\tau_1=L^2/\pi^2D$. A fit of the simulation data gives a diffusion coefficient $D=2.70$ nm²/ns. The solid curve in Fig. 3 represents the full solution [Eq. (10)] with this value of D . Likewise, the solid curve in Fig. 2 represents $F_p(t)$ [Eq. (9)] with the same diffusion coefficient. Apparently we can map the diffusive motion in the direction of the channel axis onto a one-dimensional diffusion model, with a diffusion coefficient $D=2.70$ nm²/ns. This value is considerably lower than the bulk value $D=4.25$ nm²/ns, which we obtained from a standard MSD analysis [Eq. (1)] as well as with the FPT methodology applied to a slab (see below).

An alternative way to determinate the diffusion coefficient is through the mean exit time $T(z_0)$, the time it takes a molecule to reach either boundary of the domain for the first time, starting from a given initial position $z=z_0$. The mean exit time as function of z_0 is shown in Fig. 4. The parabola is based on Eq. (7), where the value $D=2.62$ nm²/ns is determined by the requirement that the spatially averaged mean exit time $\langle T \rangle$ is equal to $L^2/12D$ [Eq. (8)]. This is approximately 3% lower than the value $D=2.70$ nm²/ns obtained from the permeation time analysis, which is in reasonable agreement. Closer inspection of Fig. 4, however, reveals an intriguing feature. The mean exit times near the domain boundaries ($z_0 \downarrow 0$ and $z_0 \uparrow L$, respectively) are on the order of 20 ps, rather than zero. This behavior is even clearer in the representation in Fig. 5, where the parabola is transformed into a straight line. We observed the same phenomenon in the FPT analysis of various bulk liquids.¹³ In those systems the geometry is a slab, rather than a channel, with dimensions of $L_x \times L_y \times L_z = 5 \times 5 \times 2$ nm³, embedded in a box of size $L_x \times L_y \times L_z = 5 \times 5 \times 10$ nm³. The delimiting planes of the slab perpendicular to the z axis act as virtual absorbing boundaries, while in the transverse (x, y) directions periodic boundary conditions are applied. We will first discuss the bulk behavior of the water model used here, and then return to that of the actual CNT system.

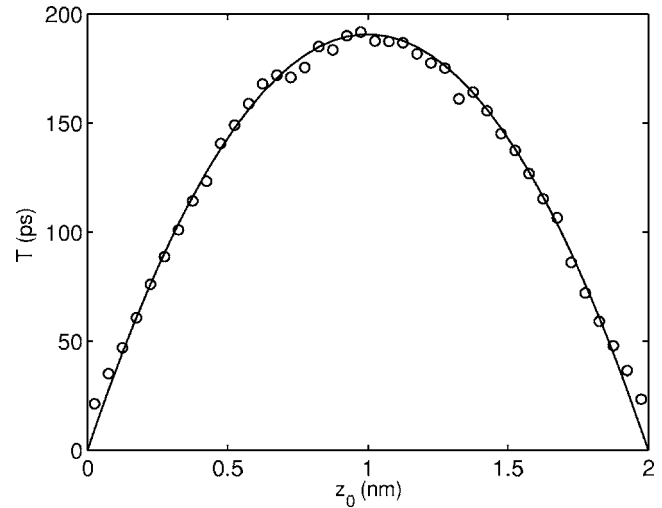


FIG. 4. Mean exit time T as function of z_0 for water inside the CNT of length $L=2$ nm. (○) Simulation. (—) Fit according to Eq. (7) with $D=2.62$ nm²/ns.

The dashed line in Fig. 5 is a linear fit to MD simulation results obtained for a slab of water of thickness $L=2$ nm. The existence of a nonzero exit time at the absorbing boundaries can be reconciled with Eq. (7) by introducing *effective* boundaries at $z=-\lambda_M$ and $z=L+\lambda_M$ respectively, with $\lambda_M=0.050$ nm. Introduction of a shifted coordinate $\tilde{z}=z+\lambda_M$ transforms Eq. (7) into

$$T(\tilde{z}_0) = \frac{1}{2D} \tilde{z}_0 (\tilde{L} - \tilde{z}_0), \quad (11)$$

with an effective channel length defined as

$$\tilde{L} = L + 2\lambda_M, \quad (12)$$

which is equal to $\tilde{L}=2.10$ nm. From the slope $1/2D$ we obtain a diffusion coefficient $D=4.25$ nm²/ns, consistent with the value obtained with a MSD analysis [Eq. (1)].

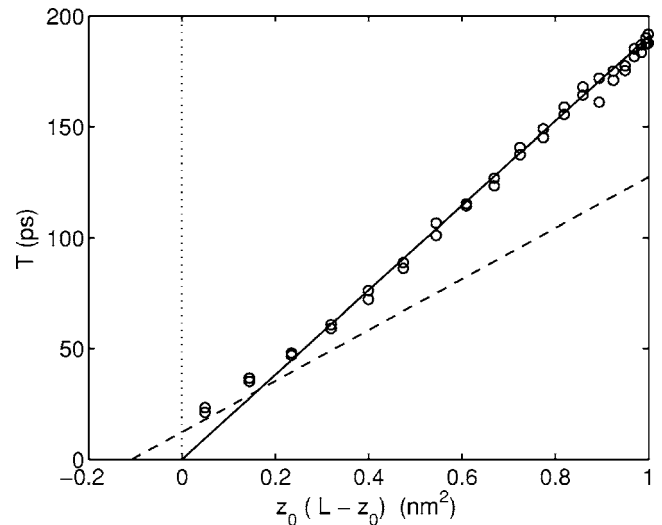


FIG. 5. Mean exit time T as a function of $z_0(L-z_0)$ for water inside a CNT of length $L=2$ nm. (○) Simulation. (—) Line with slope $1/2D$, where $D=2.62$ nm²/ns. It is equivalent to the parabola in Fig. 4. The dashed line corresponds to bulk water, with $D=4.25$ nm²/ns (data points are omitted for clarity). It crosses the horizontal axis at $-\lambda_M(L+\lambda_M)$, with $\lambda_M=0.050$ nm.

The quantity λ_M was identified¹³ as the *Milne extrapolation length*.^{14,26,27} Its value depends on the details of the molecular system, primarily the type of molecule and state variables such as temperature and pressure. It emerges because the diffusion equation [Eq. (3)] represents positions of particles only, and therefore cannot account for velocity-related phenomena explicitly. The derivation of Eq. (7) is based on the assumption that the concentration is zero at an absorbing boundary [Eq. (4)]. However, absorption implies that a molecule is not allowed to return after crossing the boundary for the first time, i.e., unidirectional (outgoing) flux rather than zero concentration is the physically correct boundary condition at the interface. This gives rise to a kinetic boundary layer, with a highly anisotropic distribution of velocities and a concentration that is nonzero at the boundary. The consequence of this layer may be appreciated by considering a semi-infinite system with one absorbing boundary at $z=0$. Suppose a concentration c_A is maintained at position $z=z_A$, where z_A is much larger than the typical width w_b of the boundary layer. If the diffusion equation [Eq. (3)], representing particle positions only, were valid, the absorbing boundary condition $c(0)=0$ applies and the steady state concentration profile in the interval $[0, z_A]$ would be $c(z)=(z/z_A)c_A$, i.e., a straight line with slope c_A/z_A . When the boundary layer is introduced, the diffusion equation would still describe the steady state situation at positions $z \gg w_b$, but the increased concentration near the boundary causes a decrease of the latter slope, which can be parametrized as $(z/\tilde{z}_A)c_A$, with $\tilde{z}_A=z_A+\lambda_M$. The extrapolated concentration profile attains a value of zero at $z=-\lambda_M$, rather than $z=0$, hence the name Milne extrapolation length. We note that a more familiar manifestation of velocity-related limitations of the diffusion equation is the initial ballistic regime of the mean square displacement, i.e., where $\text{MSD} \sim t^2$, in contrast to the diffusive (long time) regime where $\text{MSD} \sim t$.

The time constants τ_n [Eq. (6)] appearing in the various time-dependent solutions of the diffusion equation are proportional to L^2/D . Therefore, replacement of L by \tilde{L} [Eq. (12)] implies transformation of the diffusion coefficient D to $\tilde{D}=(\tilde{L}/L)^2D$, which is expected to be the proper intrinsic diffusion coefficient of the system. For the slab of bulk water discussed here, this implies an increase of D by 10%, and, indeed, the corrected value $\tilde{D}=4.25 \text{ nm}^2/\text{ns}$ corresponds to that obtained from a MSD analysis of the data. We applied similar corrections to the simulation results of various other liquids,¹³ and, invariably, these results were consistent with the MSD-based analysis.

We now return to the mean exit time of water in a CNT, as represented in Fig. 5. In contrast to bulk behavior (dashed line), the mean exit time shows distinct deviations from linearity for small values of $z_0(L-z_0)$, corresponding to initial particle positions near the boundaries. Interestingly, however, the bulk line seems to act as an asymptote. This may be understood as follows. The computational channel ($L=2 \text{ nm}$) is separated from the reservoirs by residual parts of the physical channel, each of length of 0.35 nm. This value is considerably smaller than the channel diameter (1.2 nm). Therefore, the average environment of water molecules near

the channel ends will be much more bulklike than that of those located further inwards. A molecule which has its initial position z_0 close to the boundary $z=0$ has a high probability to be absorbed by this one, rather than the one at $z=L$ (and vice versa), while excursions further into the channel prior to absorption will be on the order of z_0 . Therefore, $T(z_0)$ is expected to be close to the behavior found in a bulk environment, a conclusion which is corroborated by Fig. 5.

The exit time of a molecule is a nonlocal property, as it depends on the mobility along the full trajectory from the initial position z_0 to the exit point. An infinitesimal change of z_0 , however, results in modification of this trajectory in the vicinity of z_0 only, irrespective of details significantly further away. For a homogeneous system, where the quadratic form [Eq. (7)] for the mean exit time is valid, the effect of such a variation can be expressed as

$$\frac{\partial T(z_0)}{\partial \xi} = \frac{1}{2D}, \quad (13)$$

with $\xi \equiv z_0(L-z_0)$. Now suppose the system is inhomogeneous, but variations are sufficiently smooth to allow a description in terms of an effective spatially varying *local* diffusion coefficient $D(z_0)$. Then, as a generalization of Eq. (13), we identify the slope of T vs $z_0(L-z_0)$ with $1/2D(z_0)$, which yields a local diffusion coefficient as

$$D(z_0) = \frac{1}{2} \left[\frac{\partial T(z_0)}{\partial \xi} \right]^{-1}. \quad (14)$$

The solid line in Fig. 5 fits the simulation data fairly well in the region $z_0(L-z_0) \geq 0.3 \text{ nm}^2$. With Eq. (14) its slope gives a diffusion coefficient $D=2.62 \text{ nm}^2/\text{ns}$. This value can be interpreted as the intrinsic value for water in the CNT, sufficiently far from the channel ends. The line crosses the z_0 axis in the origin. This, however, is a fortuitous result of counteracting effects of the increase of the diffusion coefficient toward the channel ends on the one hand and the kinetic boundary layer on the other, but obviously cannot be taken as a signature of the validity of Eq. (7) for the full channel.

From the permeation time analysis, we obtained an effective diffusion coefficient for the full channel $D=2.70 \text{ nm}^2/\text{ns}$. This value is based on the uncorrected channel length $L=2 \text{ nm}$. However, due to the variation of the diffusion properties along the channel, the simple transformation from D to $\tilde{D}=(\tilde{L}/L)^2D$ to account for a kinetic boundary layer, as discussed in relation to bulk diffusion, can no longer be applied. Therefore, we consider $D=2.70 \text{ nm}^2/\text{ns}$ as a lower bound only.

B. OmpF porin

OmpF simulation results were analyzed along similar lines as applied to the CNT system. Some features of the OmpF system are distinctly different from a CNT. We used the same computational length $L=2 \text{ nm}$, but the OmpF cross section varies between approximately 0.6 nm in the central region and 1.4 nm near the (virtual) channel ends, respectively,² as opposed to the uniform CNT value of

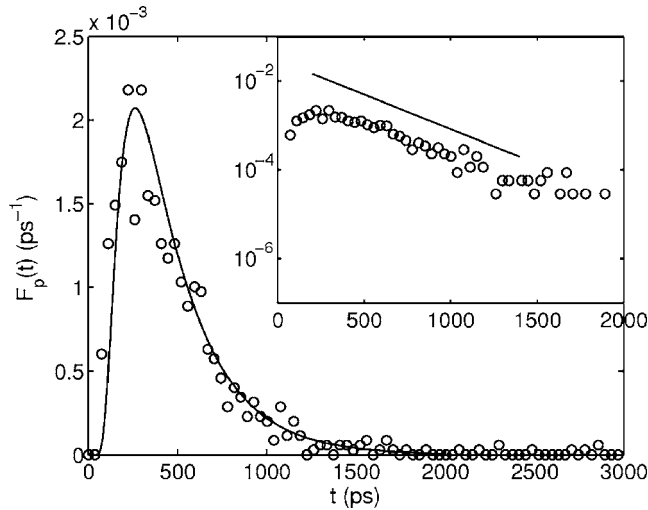


FIG. 6. Permeation time distribution $F_p(t)$ of water diffusing through an OmpF channel. The solid curve corresponds to Eq. (9), with a diffusion coefficient $D=1.35 \text{ nm}^2/\text{ns}$, obtained from the fit of $S_p(t)$ in Fig. 7. The slope of the solid line in the semilogarithmic inset corresponds to the longest time constant $\tau_1=L^2/\pi^2D$.

1.2 nm. Furthermore, the OmpF channel walls are highly heterogeneous, both chemically and in a geometrical sense.

The permeation time distribution $F_p(t)$ of water molecules traversing the monitored part of the OmpF channel is given in Fig. 6. It shows statistical fluctuations of the same order as we observed in the CNT simulations (Fig. 2). Again, this is primarily the result of the small number of molecules that contribute to the signal, as typically only $\mathcal{O}(100)$ water molecules are present in a single channel of the trimer. Likewise, the survival probability $S_p(t)$ (Fig. 7) is much less erratic. However, in contrast to Fig. 3 an additional structure is visible in the tail, starting at a survival time of about 1200 ps. The corresponding survival probability is approximately $10^{-1.5} \approx 0.03$, i.e., about 3% of the permeating particles are still present in the channel. A fit of the data in the linear intermediate time regime, say, between 400 and

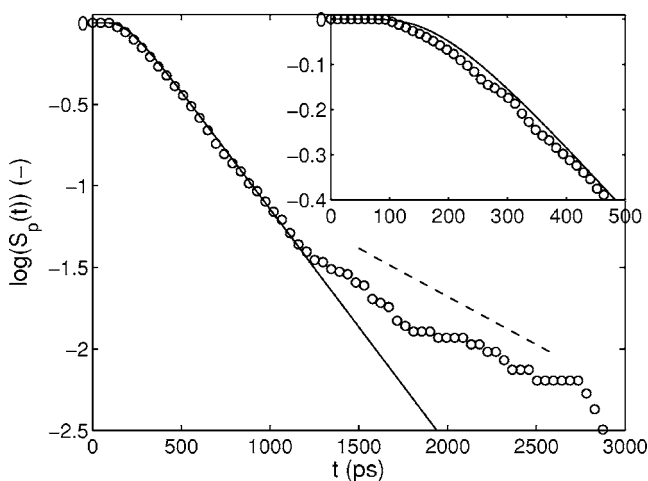


FIG. 7. Survival probability $S_p(t)$ of water permeating through OmpF. The solid curve corresponds to Eq. (9) with a diffusion coefficient $D=1.35 \text{ nm}^2/\text{ns}$. At $\log S_p(t) \approx -1.5$, a crossover to a slower exponential mode corresponding to $D' \approx 0.55 \text{ nm}^2/\text{ns}$ occurs. The dashed line corresponds to a single exponential mode with a time constant $\tau'_1=L^2/\pi^2D'$.

1000 ps, to the ($n=1$) mode of $S_p(t)$ [Eq. (10)] gives $D=1.35 \text{ nm}^2/\text{ns}$. The magnified inset reveals some deviations from the full solution at earlier times, unlike the CNT results (Fig. 3). Presumably this is caused by the highly heterogeneous character of OmpF. For survival times $t > 1200$ ps the behavior of $\log S_p(t)$ is roughly linear, but with a considerably more shallow slope than in the intermediate time regime. The governing time constant may be formally associated with a diffusion coefficient D' through $\tau'_1=L^2/\pi^2D'$, which yields a value $D'=0.55 \text{ nm}^2/\text{ns}$. This identification suggests that two “populations” of permeating particles are present, i.e., a major one with a diffusion coefficient $D=1.35 \text{ nm}^2/\text{ns}$ and a minor, much slower, one with a diffusion coefficient $D'=0.55 \text{ nm}^2/\text{ns}$. However, we visually inspected representative water trajectories with the software package VMD (Ref. 28) and found no evidence for well-separated (fast and slow) transport paths. Rather, some molecules appeared to be trapped by the protein wall of the channel for widely varying periods of time, up to the full length of the simulation run (10 ns). We note that this is quite different from the diffusion behavior of water in nanopores of a β -lactoglobulin crystal.²⁹ Here we observed two well-separated diffusion pathways with different characteristics, the first hydration layer of the protein surface on the one hand and the internal, more bulklike, region of the channel on the other.

In order to quantify this behavior, we scanned the molecular trajectories for trapping events. A molecule is considered to be trapped if the absolute displacement of its center of mass is never larger than 0.15 nm, roughly one-half of a molecular diameter, over a period $\tau > 10$ ps. The choice of the threshold value of 0.15 nm can be rationalized by considering free diffusion, i.e., between trapping periods. With a diffusion coefficient $D=1.35 \text{ nm}^2/\text{ns}$, the root mean square displacement $(2D\tau)^{1/2}$ [see Eq. (1)] over a period $\tau=10$ ps is equal to 0.16 nm. Therefore, for times $\tau \gg 10$ ps stagnation of the displacement below 0.15 nm is indicative of strongly reduced mobility. Primarily, trapping times of at least an order of magnitude longer than 10 ps are relevant for the phenomena analyzed in this work (see below). Therefore, details of the trapping detection procedure are of minor importance, and consequently we refrained from further refinement. On average, 1.7% of the water molecules appeared to be trapped. Trapping events showed no mutual correlation, i.e., after release a molecule typically returns to the “mobile region” of the channel, without preference for a next event.

Figure 8 gives the average trapping time $\langle \tau \rangle$ per trapping event as a function of the axial coordinate z , averaged over the channel’s cross section. We see a typical variation between 50 and 100 ps, with values at some positions exceeding this range considerably. The distribution of trapping times $\psi(\tau)$, irrespective of the position in the channel, is given in Fig. 9. Up to $\tau=10$ ns, the bound imposed by the run time of the simulation, it follows a power law,

$$\psi(\tau) \sim \tau^{-\mu}, \quad (15)$$

with $\mu=2.4$. This is quite different from an exponential distribution, such as we would expect if the trapping were a regular thermally activated process. Presumably this is a fin-

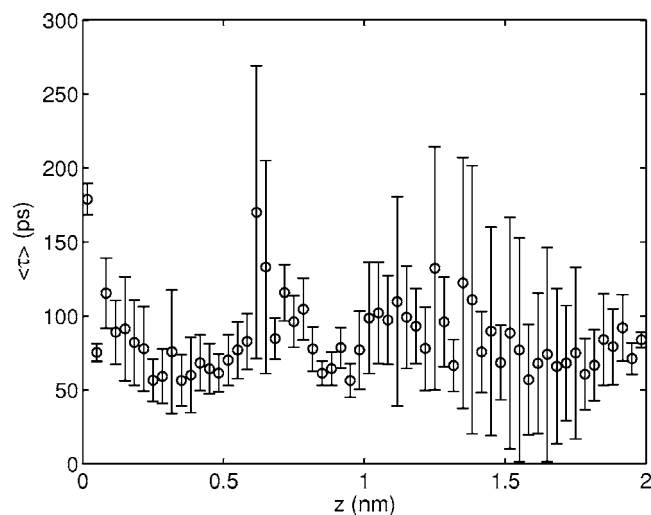


FIG. 8. Average trapping time $\langle \tau \rangle$ of water as a function of the axial position z in the OmpF channel. The error bars represent standard deviations.

gerprint of the dynamics of the protein structure. A similar distribution of trapping times was observed by Garcia and Hummer³⁰ for water in the interior of cytochrome C. Water molecules with coordination numbers not larger than 3 were considered trapped, in contrast to a typical average coordination number between 4 and 6 in the first hydration shell of molecules in a bulk environment. The occurrence of low coordination numbers is indicative of molecules being (partially) surrounded by protein components, rather than other water molecules. Simulations performed at various temperatures showed a power law [Eq. (15)], with $\mu \approx 2.5$. Both the qualitative features of the trapping behavior and the exponent μ are similar to those observed in the OmpF channel.

Trapping of water molecules in hydration layers at surfaces, rather than at localized sites, is a more frequently reported phenomenon. Here the molecules are still mobile within the layer, as opposed to the characteristics in OmpF, where the position of a trapped water molecule is essentially frozen. For several systems the distribution of residence

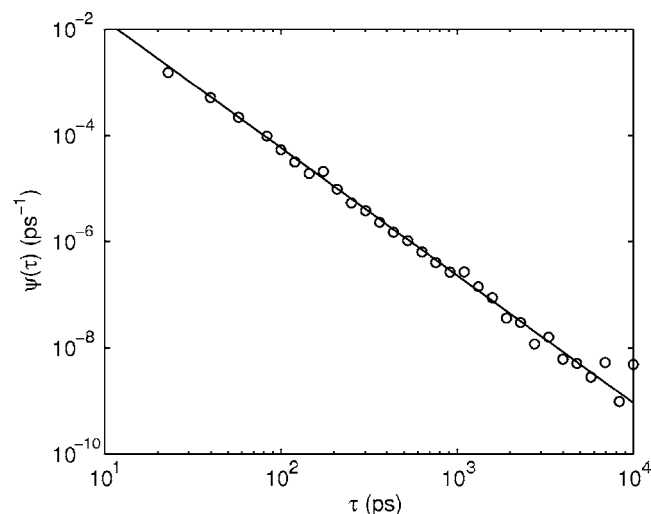


FIG. 9. Trapping time distribution $\psi(\tau)$ of water molecules inside OmpF. It follows a power law [Eq. (15)] with $\mu=2.4$, up to the run time of the simulation ($\tau=10^4$ ps).

times in a layer appears to be characterized by a power law such as Eq. (15), but with $\mu < 2$. It is attributed to long-range collective behavior of the hydrogen bond network, induced by orientational constraints imposed by the surface. The value of μ appears to depend on the thickness of the monitored layer. A typical example is water in hydration layers around plastocyanin,³¹ where exponents $\mu=1.7$, $\mu=1.5$, and $\mu=1.3$ were found for layers with thicknesses of 4, 6, and 14 Å, respectively. Similar behavior, with $\mu \approx 1.5$, was observed for water in a 6-Å-thick layer at the wall of a cylindrical silica cavity.³² It was argued that the distribution of residence times reflects a distribution of waiting times between molecular jumps, following the power law [Eq. (15)] with the same exponent μ . As μ is smaller than 2, this should give rise to subdiffusive behavior within the layer,³³ where the MSD is proportional to $t^{\mu-1}$, rather than t [Eq. (1)]. Indeed such characteristics were found in the simulations.

The diffusion coefficient D characterizes the long time translational dynamics of a molecule. It is the result of time averaging of a fluctuating environment as the particle follows a trajectory. Different trajectories represent different realizations of these fluctuations or, in other words, an ensemble of paths in phase space. The duration of a trajectory from its initiation to an absorbing boundary sets an “observation time” of the diffusion process. In our analysis this would be either the exit time from an initial axial position z_0 or the permeation time, with the simulation time of 10 ns as upper bound. Only if the observation time is sufficiently long to allow a phase point to visit a representative part of phase space, the diffusive behavior is properly represented (statistically) by the trajectory. Assuming ergodicity, an ensemble average over multiple paths in phase space would then be equal to the long-time average and hence reproduce the sought after effective diffusion coefficient. The distribution of trapping times (Fig. 9), however, indicates that this condition may not be met. Trapping times exceeding typical observation times by more than an order of magnitude are present, albeit with low probability. Therefore, these excessive trapping events represent regions in phase space which are not visited by the majority of the trajectories. This is an example of “broken ergodicity.”³⁴ The apparent emergence of a second diffusion coefficient in the survival probability (Fig. 7) suggests that the current system might be described *effectively* in terms of two subensembles, with well-separated time scales. We did not pursue a further, quantitative, analysis of these ideas, primarily due to the limited amount of data available.

Related to this discussion, we conjecture that the spatial variation of the average trapping time $\langle \tau \rangle$ (Fig. 8) does not necessarily reflect intrinsic properties of the channel. Typically, the number of trapping events contributing to a particular data point is of the order of 1500 or less. This is a rather low number, considering the wide range of time scales of $\psi(\tau)$ (Fig. 9). Therefore, the structure in Fig. 8 may primarily represent statistical fluctuations, as a result of insufficient sampling of the trapping time distribution. Of course, spatial variation of the intrinsic characteristics of the various trapping sites cannot be ruled out beforehand.

If sampling of $\psi(\tau)$ by the diffusing molecules were suf-

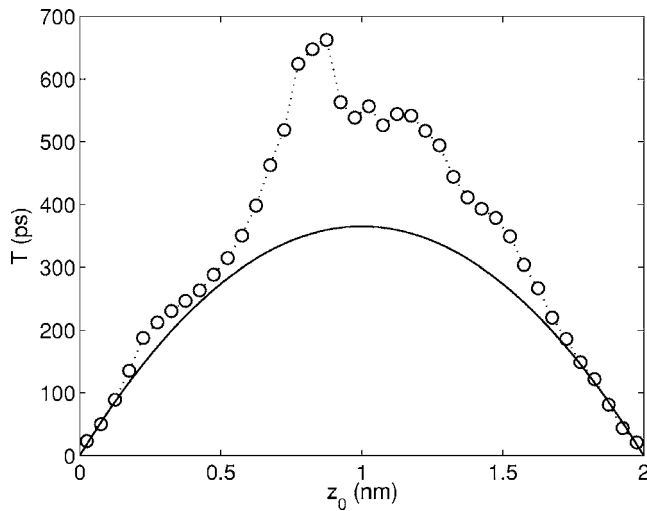


FIG. 10. Mean exit time T of water as function of the initial axial position in the OmpF channel. The solid curve (—) corresponds to Eq. (7) with a diffusion coefficient $D=1.35 \text{ nm}^2/\text{ns}$, which characterizes 97% of the permeating trajectories. The dotted curve connecting the data points is included as a guide to the eye.

ficiently representative, the effect of trapping would merely be a reduction of the diffusion coefficient according to

$$D = [1 + \langle \tau \rangle / \langle \tau_f \rangle]^{-1} D_0, \quad (16)$$

where D_0 is the diffusion coefficient if trapping were absent and $\langle \tau_f \rangle$ is the average time a particle diffuses freely between two consecutive trapping events. Here the value of the power law exponent of $\psi(\tau)$ [Eq. (15)] plays a key role. Since $\mu = 2.4$, which is larger than 2, trapping results in normal diffusion. On the other hand, $\mu \leq 2$ would result in subdiffusive behavior,³³ a phenomenon quoted earlier in connection with diffusion of water in layers close to surfaces.

The mean exit time T as function of the initial position z_0 gives additional support for our analysis. The data points in Fig. 10 show remarkable deviations from a parabola, unlike the CNT results (Fig. 4). As deduced from Fig. 7, however, the diffusion behavior of the majority of the permeating particles can be reasonably characterized by a single diffusion coefficient $D=1.35 \text{ nm}^2/\text{ns}$. Therefore, a plot of the theoretical expression for $T(z_0)$ [Eq. (7)] corresponding to this value is displayed in Fig. 10 as well. This parabola is based on a uniform diffusion coefficient throughout the channel, so deviations of $T(z_0)$ from this curve are to be foreseen, even merely due to spatial variations of the diffusive properties. However, we would expect these to be of a much smoother nature than apparent in Fig. 10. Again, we interpret this by invoking incomplete sampling of phase space. The molecules which follow “regular” permeation undergo only moderate trapping, which is accounted for in $D=1.35 \text{ nm}^2/\text{ns}$, according to Eq. (16). The mean exit time is no larger than the maximum value $L^2/8D=370 \text{ ps}$. Trapping times, on the other hand, span a range of values up to 10^4 ps (Fig. 9). Therefore, the contribution to $T(z_0)$ from a single molecule which experiences excessive trapping somewhere along its trajectory may be relatively large. This would result in a peak at z_0 relative to the surrounding positions. On the other hand, MD trajectories are sampled from multiple time origins, so a

single extreme trapping event influences the mean exit times at multiple values of z_0 and the effect on $T(z_0)$ is smeared out, but it will still stand out from the smoother global behavior. Due to incomplete sampling of the trapping time distribution $\psi(\tau)$, such extreme events are not uniformly distributed. Therefore, clear fingerprints of their presence will still be visible in $T(z_0)$ after averaging over the full simulation. This would explain the irregular structure of $T(z_0)$ in Fig. 10.

As argued earlier, we cannot rule out variations of the intrinsic properties of trapping sites as an additional source of deviations from homogeneous behavior. Further insight would require a site-specific trapping analysis, for example, along the lines of Garcia and Hummer³⁰ in their study of cytochrome C.

Zooming in on $T(z_0)$ near the channel ends, at 0 and 2 nm, respectively, shows the effect of a kinetic boundary layer, similar to the observations in the CNT analysis (Fig. 4). Given the strong deviations from a parabola, however, an attempt to perform a more detailed analysis would have little significance.

V. DISCUSSION AND CONCLUSIONS

The initial motivation for this work was to make a transition from local diffusive properties of water in OmpF to characterization of global, full-channel, behavior. To this end we explored the merits of a first passage time analysis, which, by definition, is suitable for the analysis of such a finite region in space. We analyzed the survival probability of permeating particles $S_p(t)$. Its dominant behavior could be characterized by a single effective diffusion coefficient $D = 1.35 \text{ nm}^2/\text{ns}$. This implies monoexponential asymptotic behavior, governed by a time constant $\tau_1 = L^2 / \pi^2 D$, where L is the channel length. However, at a residence time of approximately 1200 ps, we observed a crossover to a region characterized by a longer time constant, $\tau'_1 = L^2 / \pi^2 D'$, with a diffusion coefficient $D' \approx 0.55 \text{ nm}^2/\text{ns}$. This “slower” region of $S_p(t)$ represents only 3% of the permeating molecules. We attributed the emergence of a reduced diffusion coefficient to trapping of water molecules by the protein channel wall. The trapping time distribution appears to follow a power law $\psi(\tau) \sim \tau^{-2.4}$ over four decades, up to 10 ns, the length of the simulation run. Clearly, the tail of this distribution is not sampled by the majority of the molecules, since typical permeation times are well below 1000 ps. We conjectured that the presence of contributions from the tail of $\psi(\tau)$ in only a small subset of the trajectories is responsible for the occurrence of an effective slower mode of $S_p(t)$. In other words, a region of phase space corresponding to excessive trapping times is insufficiently sampled, i.e., the time average of the fluctuating environment of permeating molecules is not equivalent to an ensemble average. This concept is known as broken ergodicity.³⁴ Whereas long trapping times are rare events, the “fat tail” of $\psi(\tau)$ renders their importance considerably higher than would be the case with, e.g., a Gaussian distribution. We see this as a key characteristic, which gives rise to the observed bimodal behavior, rather than an overall reduction of the diffusion coefficient.

Tieleman and Berendsen² determined for OmpF profiles

of the components of the “local diffusion tensor” as a function of the axial position z , using a MSD analysis along the lines summarized in the Introduction. Typically, the axial diffusion coefficient varied between approximately 0.8 and 2 nm²/ns over the region of interest ($L=2$ nm). As the regular SPC water model was used, rather than the modified one as in our simulations, a direct comparison of these results with our findings is not valid. However, let us heuristically scale these values with the ratios of the bulk diffusion coefficients at 310 K for the respective water models. The reported bulk value for SPC is $D=5.1$ nm²/ns, while $D=4.25$ nm²/ns for our model. Hence, the conversion factor is $4.25/5.1=0.83$, and consequently the range of the diffusion coefficient would be $0.65 \leq D \leq 1.65$ nm²/ns. This is consistent with the effective diffusion coefficient $D=1.35$ nm²/ns extracted from our simulations.

The permeation behavior of water in a CNT exhibited no anomalies, indicative of the homogeneous character of this system. However, the mean exit time $T(z_0)$ revealed deviations from ideal behavior near the channel ends. We identified this as a transition toward bulk properties. Moreover, the effect of a kinetic boundary layer appeared. This phenomenon, which may be accounted for by effectively moving the absorbing boundaries outwards by a Milne extrapolation length λ_M , is discussed by us in more detail elsewhere.¹³

As discussed in Sec. III the diffusion coefficient D extracted from the MD simulations is the *self*-diffusivity. Therefore, the consequences of our results for *transport* diffusion through OmpF channels are not straightforward. Differences may arise if interparticle correlations play a significant role. The trapping behavior of water at the channel wall, however, does not seem to be related to such correlations. Therefore, our findings are expected to be of value to a better understanding of transport properties of OmpF as well.

The first passage time methodology presented in this paper has disclosed hitherto unnoticed properties of water diffusing through OmpF channels. In a more general sense, the results illustrate its potential as a versatile approach to the analysis of diffusion in heterogeneous systems.

ACKNOWLEDGMENTS

Support for A. J. Dammers from the Deutsche Forschungsgemeinschaft under Priority Program SPP 1155 “Molecular Modelling and Simulation in Chemical Engineering” is gratefully acknowledged. One of the authors (K.M.) was supported by the LifeTech program of Delft University of Technology. Two of the authors (V.J.v.H. and M.-O.C.)

were partially supported by the Dutch National Foundation for Scientific Research, NWO, via a PIONIER award.

- ¹S. W. Cowan, T. Schirmer, G. Rummel, M. Steiert, R. Ghosh, R. A. Pauptit, J. N. Jansonius, and J. P. Rosenbusch, *Nature (London)* **358**, 727 (1992).
- ²D. P. Tieleman and H. J. C. Berendsen, *Biophys. J.* **74**, 2786 (1998).
- ³W. Im and B. Roux, *J. Mol. Biol.* **319**, 1177 (2002).
- ⁴W. Im and B. Roux, *J. Mol. Biol.* **322**, 851 (2002).
- ⁵E. Lindahl and O. Edholm, *Phys. Rev. E* **57**, 791 (1998).
- ⁶M. Sega, R. Vallauri, and S. Melchionna, *Phys. Rev. E* **72**, 041201 (2005).
- ⁷S. T. Cui, *J. Chem. Phys.* **123**, 054706(4) (2005).
- ⁸G. R. Smith and M. S. P. Sansom, *Biophys. Chem.* **79**, 129 (1999).
- ⁹P. Ahlström, O. Teleman, and B. Jönsson, *J. Am. Chem. Soc.* **110**, 4198 (1988).
- ¹⁰P. Liu, E. Harder, and B. J. Berne, *J. Phys. Chem. B* **108**, 6595 (2004).
- ¹¹T. Munakata and Y. Kaneko, *Phys. Rev. E* **47**, 4076 (1993).
- ¹²S. Redner, *A Guide to First-Passage Processes* (Cambridge University Press, 2001).
- ¹³A. J. Dammers, V. J. van Hijkoop, and M.-O. Coppens, (unpublished).
- ¹⁴K. M. Case and P. F. Zweifel, *Linear Transport Theory* (Addison-Wesley, Reading, Massachusetts, 1967).
- ¹⁵D. van der Spoel, E. Lindahl, B. Hess, G. Groenhof, A. E. Mark, and H. J. C. Berendsen, *J. Comput. Chem.* **26**, 1701 (2005).
- ¹⁶K. A. Feenstra, B. Hess, and H. J. C. Berendsen, *J. Comput. Chem.* **20**, 786 (1999).
- ¹⁷D. van der Spoel, P. J. van Maaren, and H. J. C. Berendsen, *J. Chem. Phys.* **108**, 10220 (1998).
- ¹⁸J. T. Frey and D. J. Doren, TubeGen 3.3 web-interface, University of Delaware, Newark DE, 2005, <http://turin.nss.udel.edu/research/tubegenonline.html>.
- ¹⁹A. W. Schüttelkopf and D. M. F. van Aalten, *Acta Crystallogr., Sect. D: Biol. Crystallogr.* **60**, 1355 (2004).
- ²⁰H. M. Berman, J. Westbrook, Z. Feng, G. Gilliland, T. N. Bhat, H. Weissig, I. N. Shindyalov, and P. E. Bourne, *Nucleic Acids Res.* **28**, 235 (2000).
- ²¹H. J. C. Berendsen, J. P. M. Postma, W. F. van Gunsteren, A. DiNola, and J. R. Haak, *J. Chem. Phys.* **81**, 3684 (1984).
- ²²J. Crank, *The Mathematics of Diffusion* (Clarendon, Oxford, 1975).
- ²³A. Berezhkovskii and G. Hummer, *Phys. Rev. Lett.* **89**, 064503 (2002).
- ²⁴F. Zhu, E. Tajkhorshid, and K. Schulten, *Phys. Rev. Lett.* **93**, 224501 (2004).
- ²⁵A. Striolo, A. A. Chialvo, K. E. Gubbins, and P. T. Cummings, *J. Chem. Phys.* **122**, 234712 (2005).
- ²⁶M. A. Burschka and U. M. Titulaer, *J. Stat. Phys.* **25**, 569 (1981).
- ²⁷T. W. Marshall and E. J. Watson, *J. Phys. A* **20**, 1345 (1987).
- ²⁸W. Humphrey, A. Dalke, and K. Schulten, *J. Mol. Graphics* **14**, 33 (1996).
- ²⁹K. Malek, T. Odijk, and M.-O. Coppens, *Nanotechnology* **16**, S522 (2005).
- ³⁰A. E. Garcia and G. Hummer, *Proteins* **38**, 261 (2000).
- ³¹C. Rocchi, A. R. Bizzarri, and S. Cannistraro, *Phys. Rev. E* **57**, 3315 (1998).
- ³²P. Gallo and M. Rovere, *J. Phys.: Condens. Matter* **15**, 7625 (2003).
- ³³J.-P. Bouchaud and A. Georges, *Phys. Rep.* **195**, 127 (1990).
- ³⁴R. G. Palmer, *Adv. Phys.* **31**, 669 (1982).